ELSEVIER

Journal of Alloys and Compounds 424 (2006) 218–224

Journal of ALLOYS AND COMPOUNDS

www.elsevier.com/locate/jallcom

Effect of Co content on the structure and electrochemical properties of $La_{1.5}Mg_{0.5}Ni_{7-x}Co_x$ ($x = 0$, 1.2, 1.8) hydrogen storage alloys

Faliang Zhang [a], Yongchun Luo [b,*], Kai Sun [c], Dahui Wang [a], Ruxu Yan [a], Long Kang [a], Jianhong Chen [a]

[a] *Department of Materials Science and Engineering, Lanzhou University of Science & Technology, Lanzhou 730050, PR China*
[b] *State Key Laboratory of Advanced Non-Ferrous Materials, Lanzhou 730050, PR China*
[c] *China Institute of Atomic Energy, Beijing 102413, PR China*

Received 11 May 2005; accepted 17 October 2005
Available online 3 March 2006

Abstract

$La_{1.5}Mg_{0.5}Ni_{7-x}Co_x$ ($x = 0$–1.8) hydrogen storage alloys have been prepared by induction melting followed by an annealing treatment. X-ray diffraction (XRD) and electron probe microanalysis (EPMA) show that all of the alloys consist of a main phase with Ce_2Ni_7-type structure with small impurities, such as $LaNi_5$-type and $PuNi_3$-type phases. The combination of X-ray and neutron diffraction data shows that Mg atoms are located only at the Laves unit and that Co atoms are located only at the $CaCu_5$ unit of the Ce_2Ni_7-type unit cell. As Co content increased, the lattice parameters and cell volume increase and the hydrides become more stable. Electrochemical analyses show that all the alloys have a large discharge capacity (above 390 mAh/g) and can be easily activated by three cycles. However, the cyclic stability of the alloy electrodes becomes worse as Co content increased, which could be mainly attributed to the distribution of Co atoms in the Ce_2Ni_7-type unit cell. The $La_{1.5}Mg_{0.5}Ni_{7.0}$ alloy exhibits better cyclic stability ($S_{70}\% = 84.7$) and a higher rate dischargeability ($HRD_{900}\% = 92.32$). Electrochemical analyses show that the control process of alloy electrode reaction is hydrogen diffusion in bulk of alloy.

Keywords: Hydrogen storage alloy; Ce_2Ni_7-type structure; Electrochemical properties; Rietveld refinement

1. Introduction

Hydrogen storage alloys have been the focus of a great deal of research in the last decades because of their excellent hydrogen storage performance and environment compatibility [1,2]. Depending on the differences of crystal structure, hydrogen storage alloys AB_n (A, rare earth element or alkaline element; B, transition metal) can be mainly classified into six types: AB_5 ($CaCu_5$ type), A_2B_7 (Ce_2Ni_7 type), AB_3 ($PuNi_3$ type), AB_2 (Laves phase), AB (CsCl type) and A_2B (Mg_2Ni type) [3]. Among these, extensive research in AB_5-type and AB_2-type alloys has led to the commercialization of the nickel-metal hydride (Ni-MH) battery [4,5]. However, AB_5-type alloy electrodes exhibit low discharging capacity (about 300 mAh/g), while AB_2-type alloy electrodes are activated slowly and contain poisonous vanadium element, which limit the extensive application of both kinds of alloys.

Recently, La–Mg–Ni based alloys with $PuNi_3$-type structure have attracted considerable attention as negative materials of Ni-MH battery systems in view of their higher discharge capacity when compared to that of AB_5-type alloy electrodes [6]. It is well known that the crystal structure of $PuNi_3$-type alloy is obtained by combining the AB_5 and AB_2 unit [$AB_5 + 2(AB_2) = 3(AB_3)$] along c axis [7], and the magnesium is located only at AB_2 unit [8]. Liao et al. [9] reported the electrochemical properties of $La_xMg_{3-x}Ni_9$ alloy electrodes with a $PuNi_3$-type structure in which the La_2MgNi_9 alloy electrode exhibited the highest discharge capacity (397.5 mAh/g). For the La_2MgNi_9 alloy [$LaNi_5 + 2(La_{0.5}Mg_{0.5})Ni_2 = La_2MgNi_9$], about half of the lanthanum atoms in the Laves unit were substituted with magnesium atoms. However, this kind of alloy electrode exhibits poor cyclic stability; furthermore, substitution of lanthanum or nickel with other rare earth elements or other transition metals had not obviously improved the cyclic stability [10–14]. On the

* Corresponding author. Tel.: +86 931 2976 571; fax: +86 931 280 6962.
E-mail address: luoyc@lut.cn (Y. Luo).

0925-8388/$ – see front matter © 2006 Elsevier B.V. All rights reserved.
doi:10.1016/j.jallcom.2005.10.095

other hand, Kohno et al. [15] studied hydrogen storage properties of new ternary system alloys: La_2MgNi_9, $La_5Mg_2Ni_{23}$ and La_3MgNi_{14}. As a result, the $La_5Mg_2Ni_{23}$ alloy electrode showed a large discharge capacity (410 mAh/g) and perfect cyclic stability within 30 cycles. However, the details of the phase structure and the crystal structure about $La_5Mg_2Ni_{23}$ alloy have not been reported until now. To my knowledge, there is little information available in literature about $La_5Mg_2Ni_{23}$-type structure, but it is sure that the La_2Ni_7 alloy with Ce_2Ni_7-type structure exists in La–Ni phase diagram [16]. In addition, Dunlap et al. [7] and Parthe and Lemaire [17] reported that Ce_2Ni_7-type structure is very similar to $PuNi_3$-type structure, and that the crystal structure of Ce_2Ni_7-type alloy can be also obtained by combining AB_5 and AB_2 units [$AB_5 + AB_2 = A_2B_7$], but the ratio between AB_5 and AB_2 unit in Ce_2Ni_7-type alloy is different from that in $PuNi_3$-type alloy. Therefore, it is necessary to study the properties of $La_{1.5}Mg_{0.5}Ni_7$ alloy with Ce_2Ni_7-type structure assuming that $La_{1.5}Mg_{0.5}Ni_7$ can be formed with a $LaNi_5 + La_{0.5}Mg_{0.5}Ni_2 = La_{1.5}Mg_{0.5}Ni_7$ formula.

It is well known that the cyclic stability of AB_5-type alloy electrodes can be improved remarkably by replacing nickel in part with cobalt, which is mainly due to the noticeable depression of the lattice expansion [18,19]. Therefore, it can be expected that the overall electrochemical properties of the $La_{1.5}Mg_{0.5}Ni_7$ alloy electrode with Ce_2Ni_7-type structure would be improved by cobalt substitution in part for nickel. Therefore, we designed the $La_{1.5}Mg_{0.5}Ni_{7-x}Co_x$ ($x = 0$, 1.2, 1.8) alloys and examined the structure and electrochemical properties.

2. Experimental

Hydrogen storage alloys with nominal composition $La_{1.5}Mg_{0.5}Ni_{7-x}Co_x$ ($x = 0$, 1.2, 1.8) were prepared by induction melting at a 0.4 MPa Ar atmosphere followed by annealing treatment between 1123 and 1223 K at a 0.2 MPa Ar atmosphere. The purity of all elements was above 99 wt%. Due to the high vapor pressure of magnesium, an appropriate excess of magnesium was necessary.

The annealed alloys were ground mechanically into powder below 400 mesh for X-ray diffraction (XRD) measurements, below 200 mesh for neutron diffraction (ND) and between 250 and 300 mesh for electrode test. The crystal structure characterization of alloys was examined by XRD measurements on a Rigaku D/max-2400 diffractometer with Cu radiation and a power of 40 kV × 100 mA. The XRD patterns were recorded over the range 15–110° in 2θ by step of 0.02°. Measurement of ND was performed on a two-axis diffractometer at China Institute of Atomic Energy in Beijing. The wavelength was set to 1.159 Å. The ND pattern was collected with 0.1° step from 10° to 100° in 2θ. Then the collected data were analyzed by the Rietveld method [20] using Fullprof 2K software [21].

The microscopic structure and the composition of $La_{1.5}Mg_{0.5}Ni_{5.8}Co_{1.2}$ and $La_{1.5}Mg_{0.5}Ni_{5.2}Co_{1.8}$ alloys were observed and analyzed by electron probe microanalysis (EPMA) using a JXA-8800R electron probe microanalyzer.

Alloy electrodes were prepared by cold pressing the mixture of alloy powder and carbonyl nickel powder at the weight ratio of 1:2 under 800 MPa pressure to form a pellet of 10 mm in diameter. Electrochemical measurements were performed at 298 K in a standard open tri-electrode electrolysis cell consisting of alloy electrode, a sintered $Ni(OH)_2$/NiOOH counter electrode and a Hg/HgO reference electrode immersed in 6 M KOH electrolyte. Each electrode was charged at 100 mA/g for 5 h and discharged at 100 mA/g until the cut-off potential of −0.6 V versus Hg/HgO reference electrode was reached. The high rate dischargeability (HRD) was determined by examining the discharge capacity at various discharge current densities. Because of low hydrogen absorption/desorption plateau for La–Mg–Ni alloy system [22], a self-discharge problem can be ignored if the time for testing of electrodes is not very long [23]. Therefore, *P–C* isotherms could be determined by electrochemical method according to the Nernst equation [24]:

$$\text{Eeq (versus Hg/HgO)} = -0.9305 - 0.02955 \log(P_{eq}) \quad \text{at } 298\text{ K} \tag{1}$$

where the equilibrium potential (Eeq) was determined by alternately performing the following operation: (1) a pulse charge/discharge of 10 mAh/g with 50 mA/g current density and (2) a rest period (about 20 min) long enough for the potential to become constant.

To investigate the electrocatalytic activity and kinetics properties of alloy electrodes, analyses of linear polarization, anodic polarization and coefficient of hydrogen diffusion in alloy bulk were performed using a CHI600A elec-

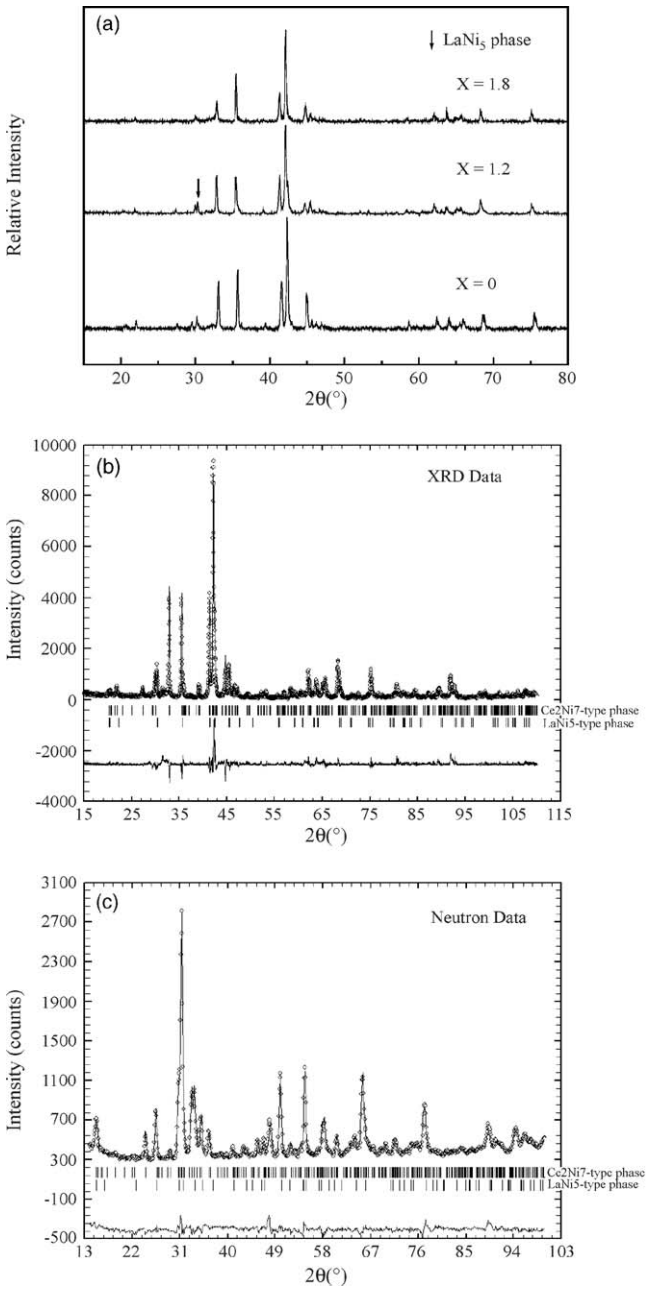

Fig. 1. Diffraction patterns of $La_{1.5}Mg_{0.5}Ni_{7-x}Co_x$ ($x = 0$–1.8) alloys: (a) XRD patterns for $La_{1.5}Mg_{0.5}Ni_{7-x}Co_x$ ($x = 0$–1.8) alloys, (b) Rietveld refinement pattern with XRD data for $La_{1.5}Mg_{0.5}Ni_{5.8}Co_{1.2}$ alloy and (c) Rietveld refinement pattern with ND data for $La_{1.5}Mg_{0.5}Ni_{5.8}Co_{1.2}$ alloy.

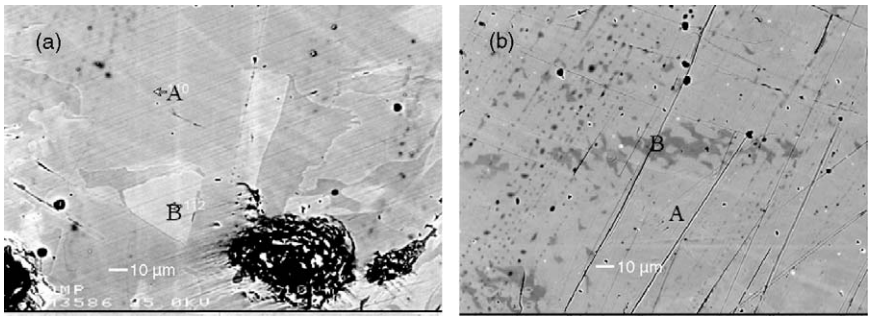

Fig. 2. Back scattering electron images for $La_{1.5}Mg_{0.5}Ni_{5.8}Co_{1.2}$ alloy (a) and $La_{1.5}Mg_{0.5}Ni_{5.2}Co_{1.8}$ alloy (b).

trochemical work station after the alloy electrodes were activated. The linear polarization and anodic polarization were measured by scanning the electrode potential at a rate of 0.1 mV/s from −6 to 6 mV (versus open circuit potential) and 5 mV/s from 0 to 450 mV (versus open circuit potential), respectively, at 50% depth of discharge (DOD). The hydrogen diffusion coefficients were measured by using the constant potential-step discharge technique. The test electrodes in fully charged state were discharged at a constant potential-step of +0.6 V for 2500 s.

3. Results and discussion

3.1. Crystal structure

Fig. 1(a) shows the XRD patterns of the $La_{1.5}Mg_{0.5}Ni_{7-x}Co_x$ (x = 0–1.8) alloys, and Fig. 2 shows the back scattering electron images of x = 1.2 and 1.8 alloys. It can be seen that all alloys consisted of main phase with Ce_2Ni_7-type structure (space group $P6_3/mmc$) with small impurities, such as $LaNi_5$-type phase in the x = 1.2 alloy and $PuNi_3$-type phase in the x = 1.8 alloy. Both EPMA analysis and Rietveld refinement verified the result as shown in Fig. 1(b and c) and Table 1. From Fig. 2(a) and Table 1, it can be found that the alloy for x = 1.2 contained two different regions, region A and region B. Analysis of EPMA showed that the lanthanum content in region B was more than that in region A, while stoichiometry (Ni/(La + Mg)) for both regions was very similar. This result indicates that the homogeneity of x = 1.2 alloy was not good, which may have resulted from insufficient annealing treatment. In Fig. 2(b), a little $PuNi_3$-type phase, region B, was observed, the composition of which was $La_{0.69}Mg_{0.23}Ni_{2.28}Co_{0.72}$. However, the diffraction peaks of $PuNi_3$-type phase were not found as shown in Fig. 1(a), which may be attributed to two factors: one is the serious overlap of diffraction peaks between $PuNi_3$-type phase and Ce_2Ni_7-type phase [25], the other is a little abundance of $PuNi_3$-type phase. To clarify the distribution of Mg and Co atoms in the crystallographic cell, both X-ray and neutron diffraction data were used because the contrast of scattering factor between lanthanum and magnesium is large for X-ray diffraction, and the contrast of scattering factor between cobalt and nickel is large for neutron diffraction [26]. Fig. 1(b and c) shows the refinement patterns of X-ray diffraction and neutron diffraction, respectively, for the x = 1.2 alloy. The crystallographic parameters are tabulated in Table 2. It can be seen that Mg atoms are located only at 4f1 site in the Laves unit, and not found at 4f2 site in AB_5 unit. This kind of distribution of magnesium in Ce_2Ni_7-type alloys is very similar to that in $PuNi_3$-type alloys. It should be noted that the actual content of magnesium in x = 1.2 alloy, depending on the Rietveld and EPMA analyses, was less than the nominal expected content of magnesium, which may be related to the volatilization of magnesium during preparation process. From Table 2, it is also distinct that a part of cobalt atoms is located at the AB_5 unit, such as 6h, 4e and 4f sites, and the other part is located at the boundary between AB_5 unit and Laves unit such as the 12k site. However, cobalt atoms are not found in Laves unit such as the 2a site. The preference of cobalt for AB_5 unit may be related to the formation condition of the Laves phase. Fig. 3 gives the distribution of magnesium and cobalt in Ce_2Ni_7-type unit cell, according to the result of Rietveld analysis. As shown in Table 1, cobalt content in the x = 1.2 alloy, calculated from the Rietveld refinement, was consistent with the result of EPMA analysis, which indicates the reliability of the Rietveld analysis. However, we also noted that the error of occupancy factor, ζ, in Table 2 was not small and the R factor for the refinement of X-ray data was big, which may be attributed to the no-homogeneity of x = 1.2 alloy. Besides, according to the result of EPMA analysis as shown in Table 1, stoichiometry of every phase in alloy was a little larger than the real stoichiometry, which may be due to the existence of light element Mg and actual instrument performance.

Fig. 4 shows the variations of lattice parameters and volume as a function of x for $La_{1.5}Mg_{0.5}Ni_{7-x}Co_x$ (x = 0–1.8) alloys. As cobalt content increased, the lattice parameters and cell volume

Table 1
Lattice parameters and composition analysis for $La_{1.5}Mg_{0.5}Ni_{7-x}Co_x$ (x = 0–1.8) alloys

Alloy	Unit cell parameters				Rietveld analysis	EPMA analysis	
	a (Å)	C (Å)	C/a	V (Å^3)		Main phase (region A)	Second phase (region B)
x = 0	5.036	24.206	4.81	530.10	$La_{1.57}Mg_{43}Ni_{7.0}$	–	–
x = 1.2	5.051	24.292	4.81	537.91	$La_{1.59}Mg_{0.41}Ni_{5.7}Co_{1.3}$	$La_{1.59}Mg_{0.32}Ni_{5.8}Co_{1.2}$	$La_{1.61}Mg_{0.28}Ni_{5.80}Co_{1.20}$
x = 1.8	5.057	24.299	4.81	538.18	$La_{1.58}Mg_{0.42}(NiCo)_{7.0}$	$La_{1.56}Mg_{0.37}Ni_{5.19}Co_{1.81}$	$La_{0.69}Mg_{0.23}Ni_{2.28}Co_{0.72}$

Table 2
Crystallographic parameters for $La_{1.5}Mg_{0.5}Ni_{5.8}Co_{1.2}$ alloy with a space group $P6_3/mmc$

Atom	Symmetry	x	y	z	ζ(Mg)	ζ(Co)
(La, Mg)	4f1	0.3333	0.6667	0.0258(2)	0.41(1)	–
La	4f2	0.3333	0.6667	0.1708(2)	0	–
Ni	2a	0	0	0	–	0
(Ni, Co)	4e	0	0	0.1676(5)	–	0.23(5)
(Ni, Co)	4f	0.3333	0.6667	0.8329(4)	–	0.08(4)
(Ni, Co)	6h	0.8332(26)	1.6665(26)	0.25	–	0.24(4)
(Ni, Co)	12k	0.8313(17)	1.6625(17)	0.0844(2)	–	0.21(3)

$R_p = 3.76$ and $s = 1.08$ for ND data. $R_p = 14.7$ and $s = 1.8$ for XRD data. ζ(Mg) represents the atomic ratio of magnesium replacing lanthanum at each site. ζ(Co) represents the atomic ratio of cobalt replacing nickel at each site.

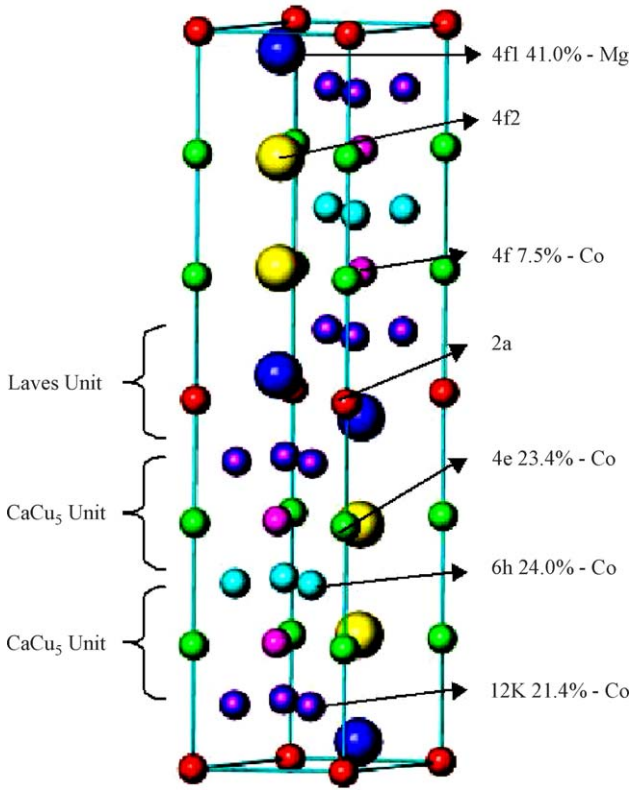

Fig. 3. Distribution pattern of Mg and Co atoms in Ce_2Ni_7-type unit cell.

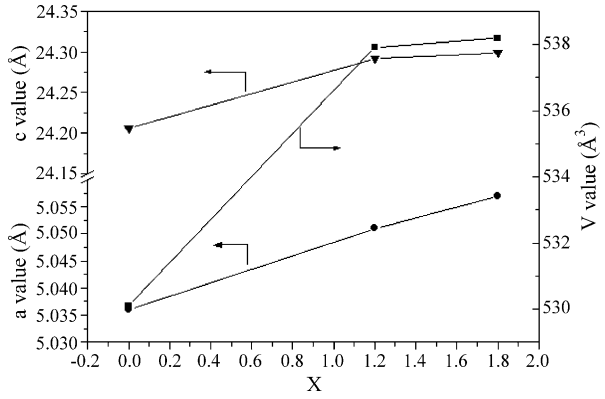

Fig. 4. Variations of lattice parameters and volume as the function of x for $La_{1.5}Mg_{0.5}Ni_{7-x}Co_x$ ($x = 0$–1.8) alloys.

increased gradually. This may be attributed to the larger atomic radius of Co (1.67 Å) than that of Ni (1.62 Å). However, the variations of Lattice parameters and volume as the function of x did not obey the linear relationship completely, which may be due to the small difference of actual magnesium content in the alloys as shown in Table 1.

3.2. Thermodynamic characteristics

Fig. 5 shows the electrochemical P–C isotherms for $La_{1.5}Mg_{0.5}Ni_{7-x}Co_x$ ($x = 0$–1.8) alloys at 298 K. It can be seen that the plateau pressure of $x = 0$ alloy was obviously higher than that of the $x = 1.2$ and 1.8 alloys, while the difference in plateau pressure between $x = 1.2$ and 1.8 alloys was small. This phenomenon may result from the unit cell volume [27], obviously the volumes of $x = 1.2$ and 1.8 alloys were larger than that of $x = 0$ alloy, while the volume difference between $x = 1.2$ and 1.8 alloys was small. All of these facts indicate that the hydrides of alloys, which contain cobalt, are more stable than the hydrides of Co-free alloys.

From Fig. 5, it can be seen that the hysteresis factor of all the alloys was not big; the hysteresis factor can be defined as:

$$H_f = \mathrm{Lg}\left(\frac{P_{abs}}{P_{des}}\right) \quad (2)$$

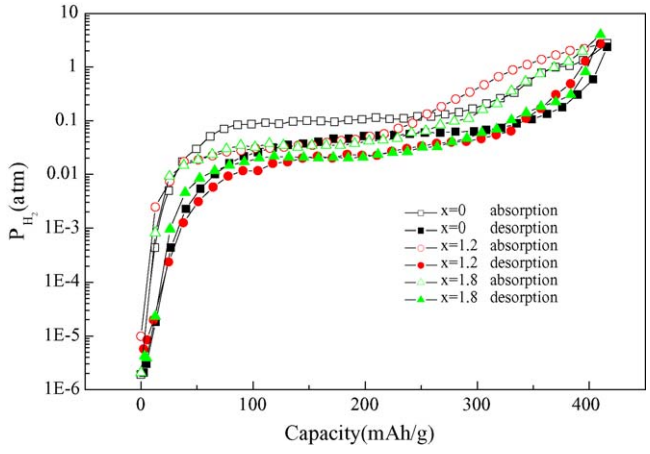

Fig. 5. Electrochemical P–C isotherms for $La_{1.5}Mg_{0.5}Ni_{7-x}Co_x$ ($x = 0$–1.8) alloy electrodes at 298 K.

Table 3
Summary of electrochemical properties for $La_{1.5}Mg_{0.5}Ni_{7-x}Co_x$ ($x = 0$–1.8) alloy electrodes

Alloy	N_a	C_{max} (mAh/g)	HRD_{900}%	S_{70}%	I_0 (mA/g)	I_L (mA/g)	D ($\times 10^{-10}$ cm^2/s)
$x = 0$	3	394.51	92.32	84.7	251.0	3900	7.8
$x = 1.2$	2	391.49	79.58	81.1	245.4	2200	3.3
$x = 1.8$	2	405.69	90.64	68.9	295.8	3210	5.7

N_a presents the cycle numbers needed to activate the electrode. S_{70}% is defined as $(C_{70}/C_{max}) \times 100$. I_0 presents the exchange current density. I_L presents the limiting current density.

where P_{abs} and P_{des} are the plateau pressure for absorption hydrogen and desorption hydrogen, respectively. Both pressures correspond to the mid point of plateaux. The H_f values for $x = 0$, 1.2 and 1.8 alloys were 0.347, 0.355 and 0.306, respectively.

3.3. Electrochemical characteristics

Table 3 summarizes the electrochemical properties of $La_{1.5}Mg_{0.5}Ni_{7-x}Co_x$ ($x = 0$–1.8) alloy electrodes. It can be seen that all of alloy electrodes could be easily activated by three cycles. What is more, the discharge capacities of all alloy electrodes ranged from 390 to 406 mAh/g, which is higher than 300 mAh/g of commercialized AB_5-type alloy electrodes [28].

Fig. 6 shows the cyclic stability curves of $La_{1.5}Mg_{0.5}Ni_{7-x}Co_x$ ($x = 0$–1.8) alloy electrodes. It can be seen that, on the one hand, an approximate linear relationship between discharge capacity and cycle number was found, which was different from cyclic stability of $La_{0.7}Mg_{0.3}Ni_{3.4-x}Mn_{0.1}Co_x$ alloy electrodes reported by Liu et al. [12]. On the other hand, as cobalt content increased, the cyclic stability of alloy electrodes became worse and the capacity retention rates of the $x = 0$, 1.2 and 1.8 alloy electrodes after 70 cycles were 84.7, 81.1 and 68.9%, respectively. It is worth noting, however, that the cyclic stability of $La_{1.5}Mg_{0.5}Ni_7$ alloy electrode with Ce_2Ni_7-type structure is much better than that of the La_2MgNi_9 alloy electrode with $PuNi_3$-type structure since the discharge capacity retention rate of the La_2MgNi_9 alloy electrode was only 60.6% after 100 cycles [22]. The difference of cyclic stability between $La_{1.5}Mg_{0.5}Ni_7$ and La_2MgNi_9 alloy electrodes is interesting for further study. It is well known that for AB_5-type alloys, cobalt is very effective to improve the cyclic stability of alloy electrodes owning to the depression of cell volume's expansion [19]. However, from Fig. 6, it indicates that the influence of cobalt on the cyclic stability for Ce_2Ni_7-type alloy electrodes and AB_5-type alloy electrodes is different, which may be due to the distribution of Co atoms in unit cell of Ce_2Ni_7-type alloy. For example, Co atoms are located only at AB_5 unit. Thus, we assume that cobalt could only depress the expansion of AB_5 unit in Ce_2Ni_7-type alloy, but not for Laves unit, it will be sure to cause more serious pulverization of alloy electrode due to their disagree expansion between AB_5 unit and Laves unit. It is also known that the discharge capacity degradation of alloy electrodes is mainly attributed to two factors: surface passivation due to the oxidation of active composition to form oxides or hydroxides and expansion of cell volume during the process of hydrogenation which leads to the pulverization of alloy particles. Pulverization accelerates the surface passivation in turn [27]. Therefore, if pulverization for Co-rich alloy electrodes is more serious, it may be the key factor leading to poor cyclic stability.

Fig. 7 shows the high rate dischargeability (HRD) of $La_{1.5}Mg_{0.5}Ni_{7-x}Co_x$ ($x = 0$–1.8) alloy electrodes. HRD can be defined as the following formula:

$$HRD = \frac{C_d}{C_d + C_{100}} \times 100\% \quad (3)$$

where C_d is the discharge capacity at the discharge current density I_d with the cut-off of -0.6 V versus Hg/HgO reference electrode; C_{100} is the residual discharge capacity when it is discharged at I_{100} current density after the electrode is discharged

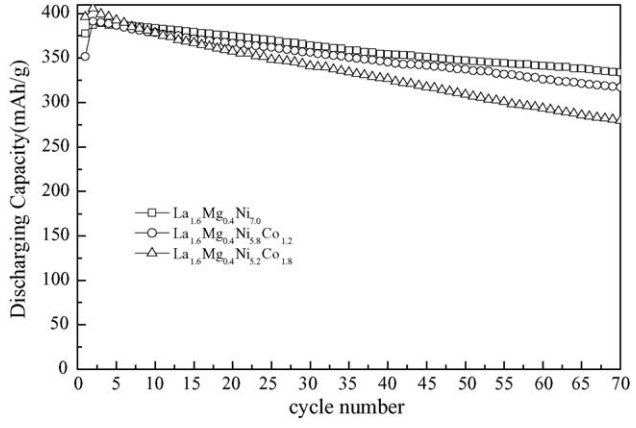

Fig. 6. Discharge capacity vs. cycle numbers for $La_{1.5}Mg_{0.5}Ni_{7-x}Co_x$ ($x = 0$–1.8) alloy electrodes at 298 K.

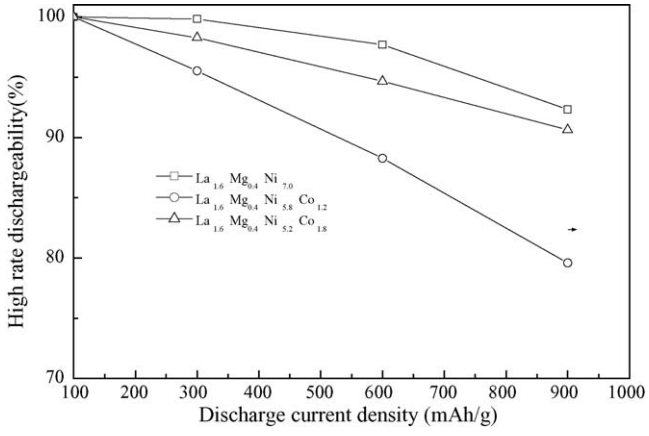

Fig. 7. High rate dischargeability (HRD) for $La_{1.5}Mg_{0.5}Ni_{7-x}CO_x$ ($x = 0$–1.8) alloy electrodes at 298 K.

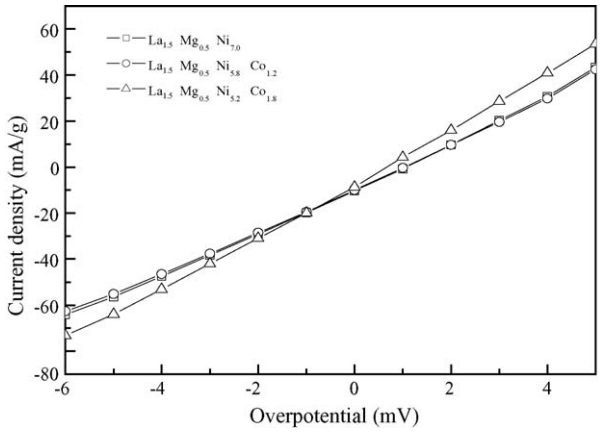

Fig. 8. Linear polarization curves for $La_{1.5}Mg_{0.5}Ni_{7-x}Co_x$ (x = 0–1.8) alloy electrodes at 50% DOD and 298 K.

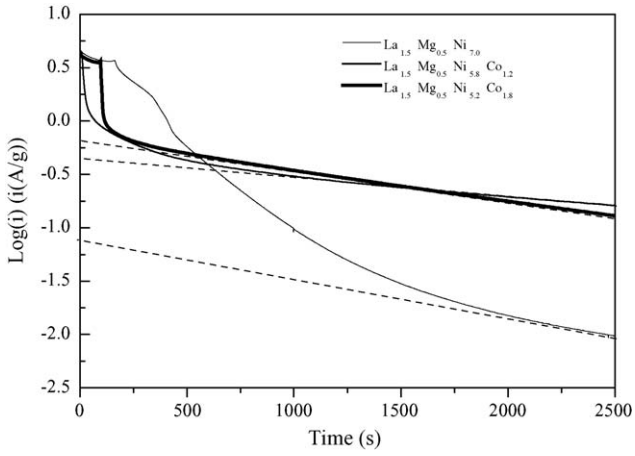

Fig. 9. Semi-logarithmic curves of anodic current vs. time responses of $La_{1.5}Mg_{0.5}Ni_{7-x}Co_x$ (x = 0–1.8) alloy electrodes at fully charged state and 298 K.

at the current density I_d. HRD can be mainly determined by two factors: charge-transfer on the electrode surface and hydrogen diffusion in the bulk of alloy [29]. Then HRD reflects overall behavior of the electrochemical kinetics of alloy electrodes. From Fig. 7 and Table 3, it can be seen that, with increasing cobalt content, HRD decreased firstly, and then increased, the Co-free alloy electrode exhibited the best HRD property ($HRD_{900}\% = 92.32$). In order to investigate the details of electrochemical kinetic properties, exchange current density (I_0), limiting current density (I_L) and hydrogen diffusion coefficient (D) were examined.

Fig. 8 shows the linear polarization curves of alloy electrodes. According to the slope, the exchange current density (I_0) can be calculated by the following formula [30]:

$$I_0 = \frac{RTI_d}{F\eta} \tag{4}$$

where R is the gas constant, T the absolute temperature, I_d the applied current density, F the Faraday constant and η is the total overpotential. It is known that I_0 is used to indicate the electrocatalytic activity of charge-transfer reaction on the surface of alloy electrodes. The I_0 values of the alloy electrodes are summarized in Table 3. The results show that the I_0 value of $x = 1.8$ alloy electrode was larger than that of $x = 0$ and 1.2 alloy electrodes, but the high rate dischargeability of $x = 1.8$ alloy electrode was not the best. In contrast, I_0 value of the $x = 0$ alloy electrode was smaller than that of $x = 1.8$ alloy electrode, but the high rate dischargeability of $x = 0$ alloy electrode was the best. All of these experimental data indicate that electrode reaction was not controlled by the charge-transfer reaction.

The coefficient of hydrogen diffusion in alloy bulk can be determined by the following equation [31]:

$$\log i = \log\left(\frac{6FD(C_0 - C_s)}{da^2}\right) - \left(\frac{\pi^2}{2.303}\right)\left(\frac{D}{a^2}\right)t \tag{5}$$

where D is the hydrogen diffusion coefficient (cm^2/s), a the radius of the alloy electrode particles (cm), I the diffusion current density (A/g) and t is the discharge time (s). Assuming that all of the alloy electrodes have the similar particle distribution with average particle radius of 14.5 μm, so according to the slope of $\log(i)$ versus t, D can be calculated. The coefficients of hydrogen diffusion (D) are listed in Table 3. Fig. 9 presents the semi-logarithmic curves of anodic current versus discharge time responses of the $La_{1.5}Mg_{0.5}Ni_{7-x}Co_x$ (x = 0–1.8) alloy electrodes. It is clear that the order of D value for different alloys was $x = 0 > x = 1.8 > x = 1.2$, which is in good agreement with the result of limiting current density (I_L) analysis as shown in Fig. 10. These experimental results indicate that Co-free alloy exhibits a bigger hydrogen diffusion than alloys which contain cobalt. It is worth noting that the order of hydrogen diffusion coefficient was consistent with that of HRD. Therefore, we can confirm that hydrogen diffusion in alloy bulk was the control step in the electrode reaction process. Besides, the smaller hydrogen diffusion coefficient of $x = 1.2$ alloy may be attributed to the lower magnesium content as shown in Table 1 because lower content of magnesium can lead to the larger cell volume, and form a more stable hydride.

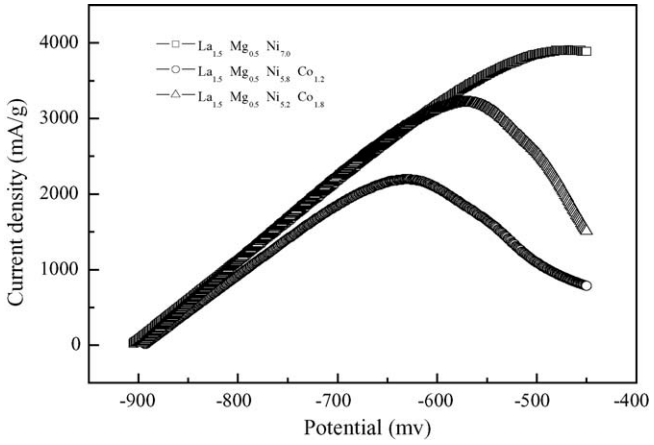

Fig. 10. Anodic polarization curves for $La_{1.5}Mg_{0.5}Ni_{7-x}Co_x$ (x = 0–1.8) alloy electrodes at 50% DOD and 298 K.

4. Conclusions

$La_{1.5}Mg_{0.5}Ni_{7-x}Co_x$ ($x = 0$–1.8) alloys with Ce_2Ni_7-type structure have been prepared successfully by induction melting followed by an annealing treatment. In the Ce_2Ni_7-type crystallographic cell, Mg atoms are located only at the Laves unit, while Co atoms only at the AB_5 unit. As cobalt content increased, the lattice parameters and cell volume become larger. The discharge capacities of all alloy electrodes surpass 390 mAh/g, and the discharge capacity of the $La_{1.5}Mg_{0.5}Ni_{5.2}Co_{1.8}$ alloy electrode reached 405.69 mAh/g. What is more, all of the alloy electrodes can be easily activated by three cycles. As cobalt content increased, the cyclic stability becomes worse, which could be mainly attributed to the distribution of Co atoms in the unit cell. The $La_{1.5}Mg_{0.5}Ni_{7.0}$ alloy electrode exhibited better cyclic stability ($S_{70}\% = 84.7$), and higher rate dischargeability ($HRD_{900}\% = 92.32$) which is due to larger hydrogen diffusion in alloy bulk. Electrochemical analysis shows that the control process of alloy electrode reaction is hydrogen diffusion in bulk of alloys.

Acknowledgement

This work was supported by the National Nature Science Foundation of China (No. 50171021) and by the academic echelon of Lanzhou University of Technology.

References

[1] J.J. Willems, Phillips J. Res. 39 (1) (1984) 1.
[2] D.G. Westlake, J. Less-Common Met. 91 (1983) 1.
[3] G. Sandrock, J. Alloys Compd. 293–295 (1999) 877.
[4] T. Sakai, M. MatsuoKa, C. Iwakura, in: L. Eyring (Ed.), Handbook on the Physics and Chemistry of Rare Earths, Elsevier, Amsterdam, 1995, p. 133.
[5] F. Feng, M. Geng, D.O. Northwood, Int. J. Hydrogen Energy 26 (2001) 725.
[6] K. Kadir, T. Sakai, I. Uehara, J. Alloys Compd. 302 (2000) 112.
[7] B.D. Dunlap, P.J. Viccaro, G.K. Shenoy, J. Less-Common Met. 74 (1980) 75.
[8] K. Kadir, T. Sakai, I. Uehara, J. Alloys Compd. 257 (1997) 115.
[9] B. Liao, Y.Q. Lei, L.X. Chen, G.L. Lu, H.G. Pan, Q.D. Wang, J. Power Sources 3 (6) (2004) 249.
[10] J. Chen, N. Kuriyama, H.T. Takashita, H. Tanada, T. Sakai, M. Haruta, Electrochem. Solid State Lett. 311 (2000) L5.
[11] C.H. Peng, M. Zhu, J. Alloys Compd. 375 (2004) 324.
[12] Y. Liu, H. Pan, M. Gao, R. Li, Y. Lei, J. Alloys Compd. 376 (2004) 296.
[13] L. Yongfeng, P. Hongge, G. Mingxia, Z. Yunfeng, L. Yongquan, W. Qidong, Int. J. Hydrogen Energy 29 (3) (2004) 297.
[14] B. Liao, Y.Q. Lei, L.X. Chen, G.L. Lu, H.G. Pan, Q.D. Wang, J. Alloys Compd. 376 (2004) 186.
[15] T. Kohno, H. Yoshida, F. Kawashima, T. Inaba, I. Sakai, M. Yamamota, M. Kanda, J. Alloys Compd. 311 (2000) L5.
[16] T. Yamamota, H. Inui, M. Yamaguchi, K. Sato, S. Fujitani, Acta Metall. 45 (1997) 5231.
[17] E. Parthe, R. Lemaire, Acta Cryst. B31 (1975) 1879.
[18] T. Sakai, K. Oguro, H. Miyamura, N. Kurigyama, A. Kato, H. Ishikawa, C. Iwakura, J. Less-Common Met. 161 (1990) 193.
[19] T. Vogit, J.J. Rellly, J.R. Johnson, G.D. Adzic, J. Mcbreen, J. Electrochem. Soc. 146 (1999) 15.
[20] R.A. Young, The Rietveld Method, first ed., IUCr, Oxford University Press, 1995.
[21] J. Rodriguez-Carvajal, Abstract of the Satellite Meeting on Powder Diffraction Congress of IUCr, Toulouse, France, 1990, p. 127 (Fullprof Program, Version 3.5d Oct 98-LLB-JRC, 1998).
[22] B. Liao, Y.Q. Lei, L.X. Chen, G.L. Lu, H.G. Pan, Q.D. Wang, J. Power Sources 129 (2004) 358.
[23] N. Cui, J.L. Luo, Electrochim. Acta 45 (2000) 3973–3981.
[24] J. Balej, Int. J. Hydrogen Energy 10 (1985) 365.
[25] K.H.J. Buschow, A.S. Van Der Goot, J. Less-Common Met. 22 (1970) 419.
[26] G.E. Bacon, Neutron Diffraction, Clarendon Press, Oxford, 1975.
[27] J.J. Reilly, in: J.O. Besenhard (Ed.), Handbook of Battery Materials, Wiley, New York, 2000.
[28] W.K. Hu, J. Alloys Compd. 289 (1999) 299.
[29] C. Iwakura, M. Matsuoka, K. Asai, T. Kohno, J. Power Sources 41 (1992) 117.
[30] P.H.L. Notten, P. Hokkeling, J. Electrochem. Soc. 138 (1991) 1877.
[31] G. Zhang, B.N. Popov, R.E. White, J. Electrochem. Soc. 142 (1995) 2695.